

Article

Ni(II) Dimers of NNO Donor Tridentate Reduced Schiff Base Ligands as Alkali Metal Ion Capturing Agents: Syntheses, Crystal Structures and Magnetic Properties

Monotosh Mondal ^{1,2}, Maharudra Chakraborty ¹ , Michael G. B. Drew ³ and Ashutosh Ghosh ^{1,*}

¹ Department of Chemistry, University College of Science, University of Calcutta, 92, A.P.C. Road, Kolkata 700 009, India; monotosh304@gmail.com (M.M.); maharudra007@gmail.com (M.C.)

² Department of Chemistry, Haldia Government Colleg, Debhog, Purba Medinipur 721657, India

³ School of Chemistry, The University of Reading, P.O. Box 224, Whiteknights, Reading RG6 6AD, UK; mgbdrew@gmail.com

* Correspondence: ghosh_59@yahoo.com; Tel.: +91-94-3334-4484; Fax: +91-33-2351-9755

Received: 22 October 2018; Accepted: 14 November 2018; Published: 21 November 2018



Abstract: Three trinuclear Ni(II)-Na(I) complexes, $[\text{Ni}_2(\text{L}^1)_2\text{NaCl}_3(\text{H}_2\text{O})]\cdot\text{H}_2\text{O}$ (**1**), $[\text{Ni}_2(\text{L}^2)_2\text{NaCl}_3(\text{H}_2\text{O})]$ (**2**), and $[\text{Ni}_2(\text{L}^3)_2\text{NaCl}_3(\text{OC}_4\text{H}_{10})]$ (**3**) have been synthesized using three different NNO donor tridentate reduced Schiff base ligands, $\text{HL}^1 = 2\text{-}[(3\text{-methylamino-propylamino)-methyl}]\text{-phenol}$, $\text{HL}^2 = 2\text{-}[(3\text{-methylamino-propylamino)-methyl}]\text{-4-chloro-phenol}$, and $\text{HL}^3 = 2\text{-}[(3\text{-methylamino-propylamino)-methyl}]\text{-6-methoxy-phenol}$ that had been structurally characterized. Among these complexes, **1** and **2** are isostructural in which dinuclear Ni(II) units act as metalloligands to bind Na(I) ions via phenoxido and chlorido bridges. The Na(I) atom is five-coordinated, and the Ni(II) atom possesses hexacoordinated distorted octahedral geometry. In contrast, in complex **3**, two -OMe groups from the dinuclear Ni(II) unit also coordinate to Na(I) to make its geometry heptacoordinated pentagonal bipyramidal. The magnetic measurements of complexes **1–3** indicate ferromagnetic interactions between dimeric Ni(II) units with $J = 3.97\text{ cm}^{-1}$, 4.66 cm^{-1} , and 5.50 cm^{-1} for **1–3**, respectively, as is expected from their low phenoxido bridging angles (89.32° , 89.39° , and 87.32° for **1–3**, respectively). The J values have been calculated by broken symmetry DFT method and found to be in good agreement with the experimental values.

Keywords: Ni^{II} dimers; sodium ion capturing; ferromagnetic coupling; magnetostructural correlation; DFT calculation

1. Introduction

During the past few decades, synthesis and characterizations of polynuclear transition metal complexes and their magnetic and electronic properties have received much attention from chemists due to their potential applications in magnetic ordering and catalytic and biological mimicking [1–9]. A common strategy for the synthesis of such polynuclear complexes is to bind the metal centers by a single atom bridge. The Schiff bases derived from diamines and salicylaldehyde derivatives are very useful for this purpose, as the phenoxido oxygen atom can connect two or three metal centers very efficiently. The literature shows that exploiting this property, various N_2O_2 or N_2O_4 donor Schiff base ligands have been used widely for the synthesis of 3d-3d', 3d-4f/5f, and 3d-ns heterometallic complexes [10–16]. On the contrary, N_2O donor tridentate Schiff base ligands are known to form mostly homonuclear complexes [17–19]. As, for example, with Ni(II), these N_2O donor ligands form diphenoxido bridged dinuclear complexes [20–22]. These complexes attracted significant attention due

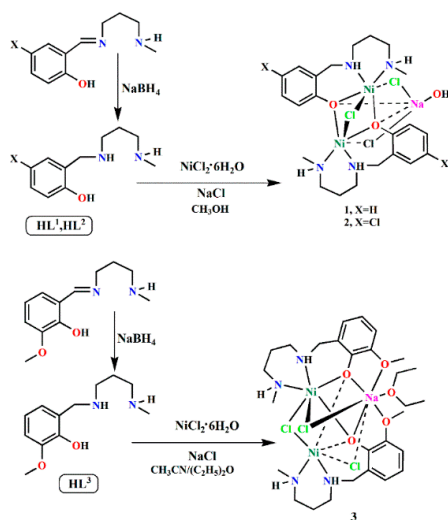
to their importance in the study of magnetic coupling between the metal centers through the phenoxido bridges [23–25]. It is now well understood that the ferro-to antiferromagnetic crossover angle for diphenoxido bridged Ni(II) is 93–94° and most of these reported complexes are antiferromagnetically coupled, because they are stable at bond angles higher than the crossover angle [26–29]. It is also known that the ferromagnetically coupled complexes with the lower Ni-O-Ni bridging angle can be obtained by introducing an additional bridging atom between the Ni(II) centers in the complexes of NNO donor ligands [23,30–33]. However, to date, unlike the mononuclear complexes of N₂O₂ or N₂O₄ donor Schiff base ligands, the dinuclear complexes of these NNO donor ligands are not known to act as metalloligands when coordinating with a second metal ion.

Herein, we report the synthesis of three new heterometallic Ni(II)-Na(I) complexes, [Ni₂(L¹)₂NaCl₃(H₂O)]·H₂O (**1**), [Ni₂(L²)₂NaCl₃(H₂O)] (**2**), and [Ni₂(L³)₂NaCl₃(OC₄H₁₀)] (**3**), by using three different NNO donor tridentate reduced Schiff bases ligands (HL¹ = 2-[(3-methylamino-propylamino)-methyl]-phenol, HL² = 2-[(3-methylamino-propylamino)-methyl]-4-chloro-phenol, and HL³ = 2-[(3-methylamino-propylamino)-methyl]-6-methoxy-phenol). The complexes are characterized by single crystal X-ray crystallography, electronic spectra, IR spectra and elemental analyses. In **1** and **2**, the sodium ion is attached to the dinuclear Ni(II) complex with the help of phenoxido and chlorido bridges, whereas in **3**, two -OMe groups form additional bridges between the dinuclear unit and Na(I). The magnetic properties of the complexes have been studied both experimentally and using broken symmetry DFT method. The couplings are found to be ferromagnetic, and consistent with the low phenoxido bridging angles between the Ni(II) centers. The experimentally obtained coupling parameters match well with the theoretically calculated values.

2. Results and Discussion

2.1. Syntheses of the Complexes

Three reduced tridentate Schiff base ligands, HL¹, HL², and HL³, were synthesized by condensation of N-methyl-1,3-propanediamine with salicylaldehyde, 5-chlorosalicylaldehyde, and 2-hydroxy-3-methoxybenzaldehyde in 1:1 molar ratios and subsequent reduction with sodium borohydride in methanol. We obtained complexes (**1–3**) accidentally in low yield when the methanolic solutions of these as-synthesized ligands were reacted directly with NiCl₂·6H₂O after reduction. The sodium ions that were present in the solution (from sodium borohydride) were captured by the dinuclear complexes. Later, in order to improve the yield, we isolated the ligands and reacted them with nickel(II) chloride in 1:1 molar ratios in the presence of sodium chloride in methanol-water solvent mixture (*vide* experimental section, Scheme 1).



Scheme 1. Synthesis of complexes **1–3**.

2.2. IR and UV–Vis Spectra of the Complexes

Complexes **1–3** show a moderately strong, sharp peak at 3266 cm^{-1} , 3270 cm^{-1} , and 3282 cm^{-1} , respectively, due to N–H stretching vibration, indicating that the imine group (C=N) of the Schiff base ligands is reduced. Absence of any sharp peak at $1620\text{--}1650\text{ cm}^{-1}$ for stretching vibration of imine group (C=N) also indicates that Schiff base is reduced (Figures S1–S3). The electronic spectra (Figure S4) of complexes **1**, **2**, and **3** are recorded in methanolic solution. The spectra show bands at 925.2 and 644.7 nm for **1**, 933.9 and 641.0 nm for **2**, and 973.7 and 638.7 nm for **3**, which can be assigned to the spin-allowed transitions ${}^3T_{1g}(F) \leftarrow {}^3A_{2g}$ and ${}^3T_{2g} \leftarrow {}^3A_{2g}$, respectively.

2.3. Description of the Crystal Structures

The structures of complexes **1** and **2**, both with the formula $[\text{Ni}_2(\text{L}^{1-2})_2\text{NaCl}_3(\text{OH}_2)]$, as shown in Figure 1 (A for **1** and B for **2**), contain crystallographic C_2 symmetry and have very similar structures. Each nickel atom is six-coordinated with a distorted octahedral environment. In the equatorial plane are three donor atoms, O(11), N(19), and N(23), of one ligand together with the oxygen atom O(11)\$1 ($\$1 = 1-x, y, 3/2-z$) of a second ligand. In axial positions there are two chlorine atoms, namely, Cl(2) on the two-fold axis, which bridges the two nickel atoms; and Cl(1), which bridges to a sodium ion, also on a two-fold axis. The sodium ion is additionally bonded to two O(11) atoms and a water molecule O(1) on the two fold axis, and thus the geometry around sodium is five-coordinated distorted trigonal bipyramidal.

The dimensions in the nickel and sodium coordination spheres in **1** and **2** are very similar and are as expected. The Ni–O(11) bonds of 2.049(2), 2.053(2) Å are shorter than the Ni–O(11)\$1 bonds of 2.164(2), 2.164(2) Å. The Ni–N bonds fall in the range of 2.079(2)–2.085(3) Å. Bonds to Cl(1) are slightly longer at 2.4782(10), 2.4626(8) Å than those to Cl(2) of 2.4300(10), 2.4497(7) Å. The sodium ions are bonded to O(11) at 2.388(3), 2.400(2) Å, and Cl(2) at 2.7532(11), 2.7525(8) Å, and O(1) at 2.293(6), 2.296(6) Å in **1** and **2**, respectively. In both structures, the water oxygen atom O(1) had high thermal parameters and the hydrogen atoms could not be located. In **1**, the atom was refined with reduced occupancy, as was an adjacent solvent oxygen atom. For both structures, there is a hydrogen bond from N(19) to Cl(2) ($\$2 = \frac{1}{2}-x, \frac{1}{2}-y, 1-z$) with dimensions H... Cl 2.61 2.56 Å, N... Cl 3.331(3), 3.332(2) Å, and N–H... Cl 130, 136° for **1** and **2**, respectively (Table 1). The Ni... Ni and Ni... Na distances are 2.963(1), 2.966(1) Å and 3.168(2), and 3.186(2) Å in **1** and **2**, respectively. In contrast, the structure of **3** that is shown in Figure 2 is different in that the ligand contains an –OMe group that is bonded to the sodium ion. However, the molecule is also located on a two-fold axis, and the arrangement around the two nickel atoms is similar to that found in **1** and **2**. The only significant difference in the bond lengths around nickel is to be found in Ni–O(11)\$1 ($\$1 = 1-x, y, 3/2-z$), which is considerably longer at 2.3178(11) Å. However the sodium ion, also on a two-fold axis, is now seven-coordinated, with a distorted pentagonal bipyramidal structure being bonded to 2*O(11), 2*O(131), and O(1) from the $(\text{C}_2\text{H}_5)_2\text{O}$ ligand in the equatorial plane at bond lengths 2.4164(15), 2.4265(13), and 2.775(4) Å, respectively. The bond to O(1) is therefore particularly weak. The five atoms in the equatorial plane show a r.m.s. deviation of 0.219 Å with the sodium ion on the two-fold axis perforce in the plane. The two chlorine atoms in axial positions form longer bonds at 2.8930(5) Å than are found in **1** and **2**. As in **1** and **2**, only one of the N–H forms a hydrogen bond, in this case N(19)–H... Cl(2)\$2 ($\$2 = -x+1/2, -y+3/2, -z+1$) with H... Cl 2.62 N... Cl 3.3454(14) Å N–H... Cl 131°. The Ni... Ni and Ni... Na distances are slightly longer than in **1** and **2** at 3.011(1), 3.280(1) Å. Selected bond lengths and bond angles are summarized in Table S1.

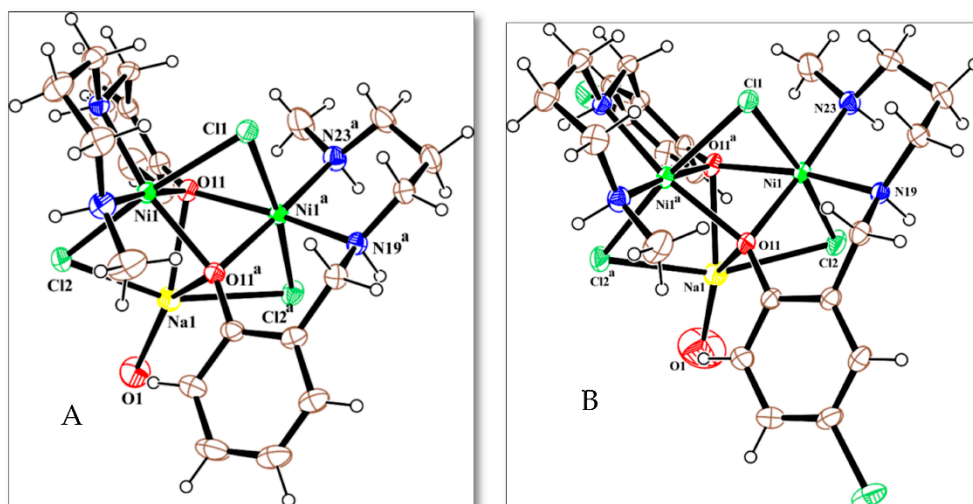


Figure 1. Structures of 1 (A) and 2 (B) with ellipsoids at 30% probability ($^a = 1-x, y, 3/2-z$).

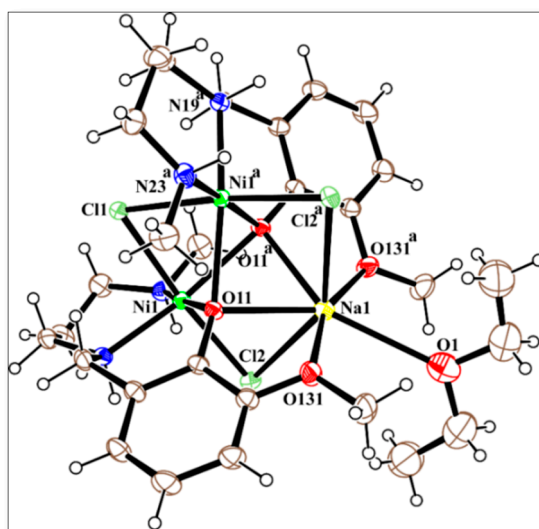


Figure 2. Structure of 3 with ellipsoids at 30% probability ($^a = 1-x, y, 3/2-z$).

Table 1. Hydrogen-Bond Parameters in Complexes (in Å and deg).

	D-H ... A	<i>d</i> (D-H)	<i>d</i> (D ... A)	<i>d</i> (H ... A)	<(D-H ... A)
Complex 1	N(19)-H(19) ... Cl(2)\$1	0.98	3.331(3)	2.61	130
Complex 2	N(19)-H(19) ... Cl(2)\$1	0.98	3.332(2)	2.56	136
Complex 3	N(19)-H(19) ... Cl(2)\$1	0.98	3.345(1)	2.62	131

In 1 and 2 \$1 = \frac{1}{2}-x, \frac{1}{2}-y, 1-z\$; in 3 \$1 = \frac{1}{2}-x, 3/2-y, 1-z\$.

2.4. Magnetic Properties

The variation of the product of molar magnetic susceptibility (χ_M) and temperature (T) with respect to temperature (T) for Ni^{II} dimers 1, 2, and 3 is presented in Figures 3–5. It can be seen that the experimental $\chi_M T$ values for three Ni^{II} dimers at room temperature (~300 K) lie around 2.24–2.73 cm³ K mol⁻¹, which in good agreement with the expected value for two non-interacting Ni^{II}, $S = 1$ centers (the theoretical spin-only value is 2.0 cm³ K mol⁻¹, $g = 2$). For all the complexes, variation of $\chi_M T$ values shows similar type of behavior on lowering the temperature: the $\chi_M T$ values gradually increase upon lowering of temperatures and attain a maximum at ca. 10–12 K. On further decreasing the temperature, a steep fall of the values is observed. This type of behavior is typical of a system that

shows dominant intramolecular ferromagnetic exchange coupling, and the steep drop in $\chi_M T$ values at lower temperatures can be attributed to zero-field splitting (ZFS) of the ground state ($S = 2$) and/or intermolecular interactions between the dimers.

The obtained magnetic data of the three compounds were analyzed by using the HDVV Hamiltonian $H = -2JS_1S_2$. We fitted the magnetic data of complexes **1**, **2**, and **3** for a simple $S = 1$ dimer model following the equation (1), which is derived from the HDVV Hamiltonian [4], in which $x = 2J/kT$.

$$\chi_M T = \frac{Ng^2\beta^2T}{k(T-\theta)} \times \frac{2e^x + 10e^{3x}}{1 + 3e^x + 5e^{3x}} \quad (1)$$

The Weiss constant was taken (θ) as an additional parameter to include the intermolecular interaction term (zJ') as well as the anisotropy term (D). The parameters N , β , and k in Equation (1) have their usual meanings, and J is the coupling parameter.

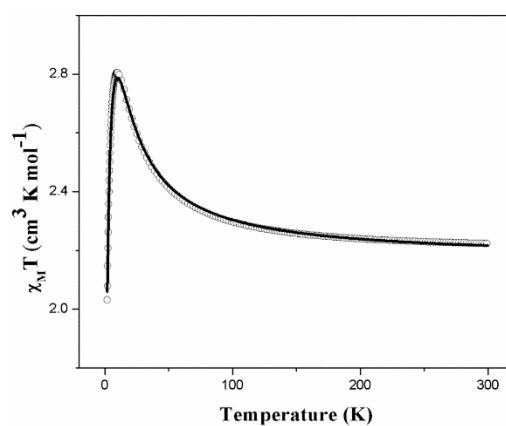


Figure 3. Plot of $\chi_M T$ vs. T for complex **1**. The circles are the experimental data, and the solid line is generated from the fitted curve.

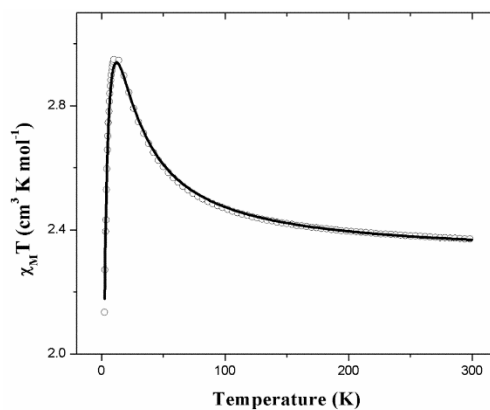


Figure 4. Plot of $\chi_M T$ vs. T for complex **2**. The circles are the experimental data, and the solid line is generated from the fitted curve.

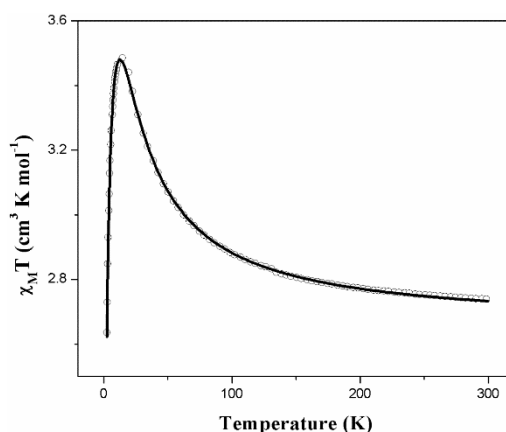


Figure 5. Plot of $\chi_M T$ vs. T for complex **3**. The circles are the experimental data, and the solid line is generated from the fitted curve.

The $\chi_M T$ versus T curves were fitted by least-squares method minimizing the function $R = \Sigma [(\chi_M T)_{\text{exp}} - (\chi_M T)_{\text{calcd}}]^2 / \Sigma (\chi_M T)_{\text{exp}}^2$. The best-fitting parameters are found to be $J = 3.97(8) \text{ cm}^{-1}$, $g = 2.08(2)$, and $\theta = -1.16 \text{ K}$ with $R = 1.2 \times 10^{-5}$ (for complex **1**); $J = 4.66(2) \text{ cm}^{-1}$, $g = 2.14(9)$, and $\theta = -1.49 \text{ K}$ with $R = 1.52 \times 10^{-5}$ (for complex **2**); and $J = 5.50(1) \text{ cm}^{-1}$, $g = 2.30(2)$, and $\theta = -1.29 \text{ K}$ with $R = 2.3 \times 10^{-6}$ (for complex **3**) (Table 2). Here, it is worth mentioning that consideration of only the anisotropy term (D) in the spin Hamiltonian yielded poor data fitting at low temperature.

Thus, besides intra-dimer coupling, ZFS and inter-dimer coupling are also present in the systems; however, their correct evaluation is not possible due to their close relationship [34,35].

Isothermal magnetization measurements studies (Figures S5–S7) suggest that the ferromagnetic coupling of all complexes leads to $S = 2$ ground spin states. However, the magnetization values at 5T are smaller than the expected values of ca. $4\mu_B$, because there are inter-dimer antiferromagnetic interactions and/or zero-field splitting [26].

Table 2. Magnetic coupling constants (J) and selective structural parameters for complexes **1**, **2** and **3**.

Complex Name	Ni–O Bond Lengths (Å)	Ni–Ni Distance (Å)	Ni–O–Ni Angle(°)	Coupling Constant (J) Theoretical (BS DFT) (cm^{-1})	Coupling Constant (J) Experimental (cm^{-1})
1	2.164(2)	2.963(1)	89.32(8)	4.25	3.97
	2.049(2)				
2	2.164(2)	2.967(1)	89.39(6)	3.56	4.66
	2.053(2)				
3	2.034(1)	3.011(1)	87.32(4)	5.50	5.50
	2.318(1)				

2.5. Theoretical Magnetic Calculation

In this present work, we have calculated the magnetic exchange parameters (J) by broken symmetry DFT calculations using B3LYP functional as described in experimental section. The Hamiltonian for the systems was taken as $H = -2JS_1S_2$, in which J is the coupling constants for the pair of Ni^{II} centers having S_1 and S_2 spin vectors for all the dimers.

The magnetic coupling constant (J) between a pair of metallic centers can be estimated by the following relationship [26]:

$$\frac{E_{\text{BS}} - E_{\text{HS}}}{S_{\text{max}}(S_{\text{max}} + 1)} = J \quad (2)$$

For complex **1**, the calculated coupling constant (J) by broken symmetry DFT method is 4.25 cm^{-1} showing ferromagnetic coupling interaction in agreement with the experimental results. However, the DFT method slightly overestimates the J value. For complex **2**, the estimated value is 3.56 cm^{-1} , which

also indicates the presence of ferromagnetic interaction between the Ni^{II} centers, but the theoretical result slightly underestimates the coupling constant. For complex **3**, the calculated value of coupling constant from broken symmetry DFT method is found to be 5.50 cm⁻¹, which is in good agreement with the experimental value.

In order to further investigate the mechanism of exchange pathway, the spin density distribution has been analyzed. Molecular orbital theory suggests that the spin delocalization transfers the spin density from the magnetic metal centers to their corresponding adjacent ligand atoms. The Mulliken spin populations of complexes **1**, **2**, and **3** in their broken symmetry states are represented in Tables 3–5, respectively (spin density orbital plots are shown in Figures S8–S10).

Table 3. The spin densities on the selected atoms for complex **1**.

Ni1	−1.626
Na1	0.000
Cl1	0.000
Cl2	−0.080
O11	−0.026
Ni1 ^a	1.626
Cl2 ^a	0.080
O11 ^a	0.026

^a Symmetry element 1−x,y,3/2−z.

Table 4. The spin densities on the selected atoms for complex **2**.

Ni1	−1.627
Na1	0.000
Cl1	0.000
Cl2	−0.079
O11	−0.024
Ni1 ^a	1.627
Cl2 ^a	0.079
O11 ^a	0.024

^a Symmetry element 1−x,y,3/2−z.

Table 5. The spin densities on the selected atoms for complex **3**.

Ni1	−1.629
Na1	0.000
Cl1	0.000
Cl2	−0.082
O11	−0.033
Ni1 ^a	1.629
Cl2 ^a	0.082
O11 ^a	0.033

^a Symmetry element 1−x,y,3/2−z.

The positive sign of spin density represents the α spin states, and the negative sign represents the β spin states. From the tables, it can be seen that two Ni^{II} centers have same amount of spin populations but the sign is opposite. Moreover, each Ni^{II} center has highest value of spin density among all the atoms present in a compound. Thus, it is obvious that Ni^{II} centers are indeed the magnetic centers. It can be also seen from the tables that about ~17% of total spin density is distributed among the other atoms present in the complexes.

If the crystallographic structure of each compound is examined, one could find two oxygen atoms and one chlorine atom bridging the two magnetic metal centers along with one Cl-Na-Cl moiety. However, we can see from the spin density table that there is nearly zero delocalization on Na and bridging Cl atom for all the complexes, and only the significant amount of spin density is

showing on the bridging oxygen atoms from phenoxido bridge. Negligible overall spin population on the bridging chloride atoms is the result of partial α and β spin density overlap due to the spin polarization in broken symmetry state (Figures S8–S10) [36–38]. Thus, it may be concluded that the ferromagnetic exchange interactions between two Ni^{II} centers are dominated by phenoxido bridges for all the complexes [39].

2.6. Comparison of Structural and Magnetic Parameters

The dimeric units of all three Ni^{II} complexes have a C₂ axis of symmetry, and the two Ni^{II} centers are connected through a pair of phenoxido bridges and a chlorido bridge along with a Cl-Na-Cl bridging unit in all the complexes (Figure 6). The core structures are similar for all the complexes, but they have slightly different Ni-O-Ni, Ni-Cl-Ni bond angles and Ni···Ni distances. From the structures of these complexes, it is expected that the overall magnetic exchange interaction between the Ni^{II} centers are mediated by two phenoxido and one chlorido bridges. However, from the spin density calculation, no significant overall spin density is observed on the chloride bridge. Thus, only the phenoxido bridges play crucial role in the coupling parameters (*J*).

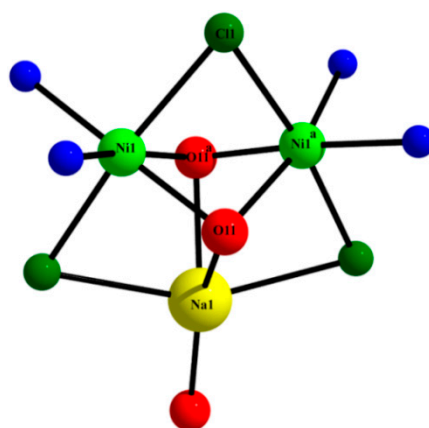


Figure 6. Environments of Ni(II) ions in complexes 1–3 with different bridging modes (phenoxido, chlorido). ^a Symmetry element 1–x, y, 3/2–z.

The sign and magnitude of the magnetic coupling constants of binuclear oxido/phenoxido bridging Ni(II) complexes have been investigated both experimentally and theoretically and correlated with the structural parameters by various groups [24,40–43]. It is now understood that ferromagnetic coupling is observed when the bridging angle is around 90° as a result of the orthogonality of magnetic orbitals. As the Ni-O-Ni angle increases, the magnitude of coupling constant decreases and tends to become antiferromagnetic at around 95°–96°. For the present complexes, the two phenoxido bridging angles are close to 90°, (89.32(8)°, 89.39(6)°, and 87.32(4)° for 1–3, respectively). Hence, the coupling is ferromagnetic. It is to be noted here that several ferromagnetically coupled diphenoxido bridged dinuclear Ni(II) were synthesized by introducing an additional water bridge between the Ni(II) centers. In the present complexes, this additional bridging atom is chloride, and it has a similar effect on magnetic coupling as the water bridge, i.e., it stabilizes the molecule below the crossover angle, and consequently the coupling becomes ferromagnetic.

3. Experimental Section

3.1. Starting Materials

Salicylaldehyde, 5-chlorosalicylaldehyde, 2-hydroxy-3-methoxybenzaldehyde and N-methyl-1,3-propanediamine, and sodium borohydride were purchased from Spectrochem, India and were of reagent grade. They were used without further purification. The other reagents and solvents were of commercially available reagent quality, unless otherwise stated.

3.2. Synthesis of the Ligands 2-[(3-Methylamino-propylamino)-methyl]-phenol (HL^1), 2-[(3-Methylamino-propylamino)-methyl]-4-chloro-phenol (HL^2), 2-[(3-Methylamino-propylamino)-methyl]-6-methoxy-phenol (HL^3)

The ligand, HL^1 , was synthesized [44] by refluxing a solution of salicylaldehyde (0.52 mL, 5 mmol) and N-methyl-1,3-propanediamine (0.52 mL, 5 mmol) in methanol (30 mL) for 1 h. The methanolic solution was subsequently cooled to 0°C and solid sodium borohydride (210 mg, 6 mmol) was added slowly with constant stirring. After completion of the addition, the resulting reaction mixture was acidified with concentrated HCl (5 mL) and then evaporated to dryness. The reduced Schiff-base ligand (HL^1) was extracted from the solid residue with methanol. This methanolic solution was used for further reaction. HL^2 and HL^3 were synthesized, maintaining a similar procedure by using 5-chlorosalicylaldehyde (782.85 mg, 5 mmol) and 2-hydroxy-3-methoxybenzaldehyde (760.75 mg, 5 mmol), respectively, instead of salicylaldehyde.

3.3. Synthesis of the Complexes $[Ni_2(L^1)_2NaCl_3(H_2O)] \cdot H_2O$ (**1**), $[Ni_2(L^2)_2NaCl_3(H_2O)]$ (**2**), and $[Ni_2(L^3)_2NaCl_3(OC_4H_{10})]$ (**3**)

$NiCl_2 \cdot 6H_2O$ (647.95 mg, 5 mmol), dissolved in 20 mL methanol, was added to methanolic solution of previously prepared HL^1 as described above with constant stirring. An aqueous solution of (2 mL) of NaCl (146.1 mg, 2.5 mmol) was slowly added with constant stirring after 15 min. The resulting green solution was kept in air for overnight. On slow evaporation of the resulting filtrate, green single crystals of complex **1** were obtained for X-ray diffraction. Complexes **2** and **3** were synthesized following the same procedure, using HL^2 and HL^3 , respectively. Green single crystals of **2** were obtained by the same procedure as stated above. For complex **3**, crystals suitable for X-ray diffraction were obtained by layer diffusion of diethylether to the acetonitrile solution of **3**.

Complex (**1**): Yield: 1.139 g; (70%). Anal. Calcd. For $C_{22}H_{36}Cl_3N_4NaNi_2O_3$ (651.31): C, 40.57; H, 5.57; N, 8.60. Found: C, 40.72; H, 5.68; N, 8.75. IR (KBr pellet, cm^{-1}): $\nu(N-H)$, 3266 cm^{-1} , $\nu(C-N)$, 1592 cm^{-1} .

Complex (**2**): Yield: 1.35 g; (75%). Anal. Calcd. For $C_{22}H_{34}Cl_5N_4NaNi_2O_3$ (720.19): C, 36.69; H, 4.76; N, 7.78. Found: C, 36.81; H, 4.90; N, 7.94. IR (KBr pellet, cm^{-1}): $\nu(N-H)$, 3270 cm^{-1} , $\nu(C-N)$, 1591 cm^{-1} .

Complex (**3**): Yield: 1.381 g; (72%). Anal. Calcd. For $C_{28}H_{48}Cl_3N_4NaNi_2O_5$ (767.46): C, 43.82; H, 6.30; N, 7.30. Found: C, 43.96; H, 6.45; N, 7.51. IR (KBr pellet, cm^{-1}): $\nu(N-H)$, 3282 cm^{-1} , $\nu(C-N)$, 1569 cm^{-1} .

3.4. Physical Measurements

Elemental analyses (C, H, and N) were performed using a Perkin-Elmer 2400 series II elemental analyzer. IR spectra in KBr pellets (4500–500 cm^{-1}) were recorded using a Perkin-Elmer RXI FT-IR spectrophotometer. Electronic spectra (1500–250 nm) were recorded in a Hitachi U-3501 spectro-photometer. The magnetic measurements of all the three Ni^{II} dimers (**1**, **2**, and **3**) were investigated with a Quantum Design superconducting quantum interference device vibrating sample magnetometer (SQUID-VSM). Powdered polycrystalline samples were used for all measurements under a DC magnetic field. The molar paramagnetic susceptibilities (χ_M) were measured at a constant magnetic field at 0.075 T under a decreasing temperature range of 300 to 2.5 K. Isothermal magnetizations measurements were performed at 2 K up to 5 Tesla for all the complexes. The measured susceptibilities were corrected according to the literature values of Pascal's table due to the diamagnetic contributions [45]. For complex **3**, all the magnetic calculations were carried out by deducting the molecular weight of readily volatile diethyl ether molecule from the actual molecular weight of the sample.

3.5. X-ray Crystallographic Data Collection and Refinement

Collected diffractable single crystals of complexes **1**, **2**, and **3** were mounted on a Bruker-AXS SMART APEX II diffractometer equipped with a graphite monochromator and Mo-K α ($\lambda = 0.71073 \text{ \AA}$)

radiation. The crystals were positioned at 60 mm from the CCD. 360 frames were measured with a counting time of 5 s. The structures were solved using direct methods with the Shelxs97 program [46]. The non-hydrogen atoms were refined with anisotropic thermal parameters. The hydrogen atoms bonded to carbon were included in geometric positions and given thermal parameters equivalent to 1.2 times those of the atom to which they were attached. The structures were refined on F^2 using Shelxl16/6 on F^2 [47]. In **1**, there were two oxygen atoms refined with reduced occupancy but the attached hydrogen atoms could not be located. For **2**, the squeeze option in Platon was used [48]. Details of the crystallographic data are summarized in Table 6. CCDC-1874587 (**1**), CCDC-1874588 (**2**), and CCDC-1874589 (**3**) contain the supplementary crystallographic data for this paper. These data can be obtained free of charge from The Cambridge Crystallographic Data Centre via www.ccdc.cam.ac.uk/data_request/cif.

Table 6. Crystallographic parameters for complexes **1**, **2** and **3**.

Compound	1	2	3
Chemical formula	C ₂₂ H ₃₆ Cl ₃ N ₄ NaNi ₂ O ₃	C ₂₂ H ₃₄ Cl ₅ N ₄ NaNi ₂ O ₃	C ₂₈ H ₄₈ Cl ₃ N ₄ NaNi ₂ O ₅
Formula weight	651.31	720.19	767.46
Crystal system	Monoclinic	Monoclinic	Monoclinic
Space group	C2/c	C2/c	C2/c
<i>a</i> (Å)	22.2673(8)	17.9326(17)	21.7316(10)
<i>b</i> (Å)	11.8915(4)	17.1847(16)	12.1574(5)
<i>c</i> (Å)	15.7543(10)	11.7063(11)	15.8456(12)
β , deg	129.106(1)	112.796(2)	126.9090(10)
<i>V</i> (Å ³)	3237.1(3)	3325.7(5)	3347.4(3)
<i>Z</i>	4	4	4
ρ_{calc} (g cm ⁻³)	1.336	1.438	1.523
μ (Mo K α) (mm ⁻¹)	1.451	1.575	1.420
<i>F</i> (000)	1352	1480	1608
Reflections collected	17,507	40,193	32,846
Independent reflections	3603	2956	3815
Reflections with <i>I</i> > 2 σ (<i>I</i>)	3031	2808	3470
<i>R</i> ₁ ^a , <i>wR</i> ₂ ^b	0.0489, 0.1745	0.0316, 0.0988	0.0269, 0.0706
<i>R</i> ₁ , <i>wR</i> ₂ [all data]	0.0572, 0.1834	0.0331, 0.1004	0.0308, 0.0705
GOF ^c	1.065	1.125	1.036
Residual electron Density, e/Å ⁻³	1.762, -0.301	0.826, -0.413	0.518, -0.378

$$^a R_1 = \frac{\sum ||F_o| - |F_c||}{\sum |F_o|}, \quad ^b wR_2 (F_o^2) = \frac{[\sum [w(F_o^2 - F_c^2)^2] / \sum w F_o^4]^{\frac{1}{2}}}{[\sum [w(F_o^2 - F_c^2)^2] / (N_{obs} - N_{params})]^{\frac{1}{2}}}$$

3.6. Computational Methodology

The Ni^{II}...Ni^{II} coupling constants (*J*) of these complexes were calculated theoretically by broken symmetry DFT as proposed by Ruiz et al. [49–51]. All the coordinates of atoms were obtained from experimental X-ray structures and used in calculations without further optimization of the structures. The hybrid B3LYP functional [52–54] along with Ahlrichs type triple zeta with polarization function def2-tzvp basis set [55] has been employed in all calculations as implemented in the ORCA package (version 3.0.3) [56]. The zero'th-order regular approximation (ZORA) has been also incorporated to describe scalar relativistic effect [57]. To speed up the calculations with desired accuracy, RIJCOSX approximation with auxiliary def2-TZVP/J coulomb fitting basis set and tight SCF convergence criteria (Grid 4) have also been incorporated [58].

4. Conclusions

In this article, three dinuclear Ni(II) complexes (**1**, **2**, and **3**) have been synthesized using the reduced form of three different NNO donor Schiff base ligands along with chloride coligand. In all the complexes, the two Ni(II) centers are connected through two phenoxido bridges and one chlorido

bridge. The additional chloride bridge reduced the Ni-O-Ni bond angles below the crossover angle, and hence ferromagnetic coupling between the Ni(II) centers was observed. These complexes are the first examples of diphenoxido bridged dinuclear Ni(II) compounds in which an additional chlorido bridge is formed between the Ni(II) centre. Moreover, these complexes provide unprecedented examples in which the dimeric Ni(II) complexes act as metalloligands to capture an alkali metal ion with the help of bridging phenoxido groups. The magnetic properties of the complexes have been rationalized by theoretical calculations. The theoretically calculated coupling parameters obtained via broken symmetry DFT methods match well with those found experimentally. Spin density calculations show that the additional chlorido bridge connecting the Ni(II) centers does not contribute to the coupling parameters and the oxo-bridges are solely responsible for the coupling by carrying the spin densities between the magnetic metal centers.

Supplementary Materials: The following are available online at <http://www.mdpi.com/2312-7481/4/4/51/s1>. Figures S1–S3: IR spectrums of complexes 1–3, Figure S4: UV-Vis spectrums of complexes 1–3, Figures S5–S7: Magnetic field dependence of molar magnetizations for complexes 1–3 at 2 K. Figures S8–S10: SD in the BS state of complexes 1–3, Table S1: Molecular dimensions (distances, Å, angles, °) in 1, 2, and 3.

Author Contributions: M.M. participated in the preparations, characterizations, X-ray structural analysis and magnetic data collections. M.C. analyzed, interpreted the magnetic data. M.G.B.D involved in structural analysis. A.G. designed the study and wrote the manuscript.

Funding: This research received no external funding.

Acknowledgments: M.C. acknowledges the financial support provided by University Grants Commission, India (F.4-2/2006 (BSR)/CH/15-16/0160, Dated 22April 2016) through the D.S. Kothari Post-Doctoral Fellowship (DSKPDF). A.G. thanks the Sophisticated Analytical Instrument Facility (SAIF), IEST, Shibpur, Howrah for providing the single crystal X-ray diffractometer facility. We also thank the CRNN, University of Calcutta, Kolkata, India, for magnetic measurement. A.G. also thanks University Grants Commission (UGC), New Delhi for funding the CAS-V, Department of Chemistry, University of Calcutta.

Conflicts of Interest: The authors declare no conflict of interest.

References

1. Deuss, P.J.; Heeten, R.; Laan, W.; Kamer, P.C. Bioinspired catalyst design and artificial metalloenzymes. *Chem. Eur. J.* **2011**, *17*, 4680–4698. [[CrossRef](#)] [[PubMed](#)]
2. Liu, W.; Thorp, H.H. Bond valence sum analysis of metal-ligand bond lengths in metalloenzymes and model complexes. 2. Refined distances and other enzymes. *Inorg. Chem.* **1993**, *32*, 4102–4105. [[CrossRef](#)]
3. Suh, J. Model studies of metalloenzymes involving metal ions as Lewis acid catalysts. *Acc. Chem. Res.* **1992**, *25*, 273–279. [[CrossRef](#)]
4. Kahn, O. *Molecular Magnetism*; VCH Publishers, Inc.: New York, NY, USA, 1993.
5. Barrios, A.M.; Lippard, S.J. Interaction of urea with a hydroxide-bridged dinuclear nickel center: An alternative model for the mechanism of urease. *J. Am. Chem. Soc.* **2000**, *122*, 9172–9177. [[CrossRef](#)]
6. Lanznaster, M.; Neves, A.; Bortoluzzi, A.J.; Szpoganicz, B.; Schwingel, E. New Fe^{III}Zn^{II} Complex Containing a Single Terminal Fe-O(phenolate) Bond as a Structural and Functional Model for the Active Site of Red Kidney Bean Purple Acid Phosphatase. *Inorg. Chem.* **2002**, *41*, 5641–5643. [[CrossRef](#)] [[PubMed](#)]
7. Borovik, A.S.; Papaefthymiou, V.; Taylor, L.F.; Anderson, O.P.; Que, L., Jr. Models for iron-oxo proteins. Structures and properties of Fe^{II}Fe^{III}, Zn^{II}Fe^{III}, and Fe^{II}Ga^{III} complexes with (.mu.-phenoxo) bis (.mu.-carboxylato) dimetal cores. *J. Am. Chem. Soc.* **1989**, *111*, 6183–6195. [[CrossRef](#)]
8. Belle, C.; Gautier-Luneau, I.; Karmazin, L.; Pierre, J.L.; Albedyhl, S.; Krebs, B.; Bonin, M. Regio-Directed Synthesis of a Zn^{II}Fe^{III} Complex from an Unsymmetrical Ligand and Its Relevance to Purple Acid Phosphatases. *Eur. J. Inorg. Chem.* **2002**, *2002*, 3087–3090. [[CrossRef](#)]
9. Mayans, J.; Font-Bardia, M.; Di Bari, L.; Arrico, L.; Zinna, F.; Pescitelli, G.; Escuer, A. From Mesocates to Helicates: Structural, Magnetic and Chiro-Optical Studies on Nickel (II) Supramolecular Assemblies Derived from Tetradentate Schiff Bases. *Chem. Eur. J.* **2018**, *24*, 7653–7663. [[CrossRef](#)] [[PubMed](#)]
10. Gheorghe, R.; Cucos, P.; Andruh, M.; Costes, J.P.; Donnadieu, B.; Shova, S. Oligonuclear 3d–4f Complexes as Tectons in Designing Supramolecular Solid-State Architectures: Impact of the Nature of Linkers on the Structural Diversity. *Chem. Eur. J.* **2006**, *12*, 187–203. [[CrossRef](#)] [[PubMed](#)]

11. Bhowmik, P.; Harms, K.; Chattopadhyay, S. Formation of polynuclear copper (II)–sodium (I) heterometallic complexes derived from salen-type Schiff bases. *Polyhedron* **2013**, *49*, 113–120. [[CrossRef](#)]
12. Biswas, S.; Naiya, S.; Drew, M.G.B.; Estarellas, C.; Frontera, A.; Ghosh, A. Trinuclear and tetranuclear adduct formation between sodium perchlorate and copper(II) complexes of salicylalimine type ligands: Structural characterization and theoretical investigation. *Inorg. Chim. Acta* **2011**, *366*, 219–226. [[CrossRef](#)]
13. Sakamoto, S.; Fujinami, T.; Nishi, K.; Matsumoto, N.; Mochida, N.; Ishida, T.; Sunatsuki, Y.; Re, N. Carbonato-Bridged $\text{Ni}^{\text{II}}_2\text{Ln}^{\text{III}}_2$ ($\text{Ln}^{\text{III}} = \text{Gd}^{\text{III}}, \text{Tb}^{\text{III}}, \text{Dy}^{\text{III}}$) Complexes Generated by Atmospheric CO_2 Fixation and Their Single-Molecule-Magnet Behavior: $[(\mu^4\text{-CO}_3)_2\{\text{Ni}^{\text{II}}(3\text{-MeOsaltN})(\text{MeOH or H}_2\text{O})\text{Ln}^{\text{III}}(\text{NO}_3)_2\}]_2$ solvent [3-MeOsaltN = N,N'-Bis (3-methoxy-2-oxybenzylidene)-1, 3-propanediaminato]. *Inorg. Chem.* **2013**, *52*, 7218–7229. [[PubMed](#)]
14. Ghosh, S.; Biswas, S.; Bauza, A.; Barceló-Oliver, M.; Frontera, A.; Ghosh, A. Use of metalloligands $[\text{CuL}](\text{H}_2\text{L} = \text{salen type di-Schiff bases})$ in the formation of heterobimetallic copper (II)-uranyl complexes: Photophysical investigations, structural variations, and theoretical calculations. *Inorg. Chem.* **2013**, *52*, 7508–7523. [[CrossRef](#)] [[PubMed](#)]
15. Thurston, J.H.; Tang, C.G.Z.; Trahan, D.W.; Whitmire, K.H. Toward Rational Control of Metal Stoichiometry in Heterobimetallic Coordination Complexes: Synthesis and Characterization of $\text{Pb}(\text{Hsal})_2$ ($\text{Cu}(\text{salen}^*)_2$, $[\text{Pb}(\text{NO}_3)(\text{Cu}(\text{salen}^*))_2](\text{NO}_3)$, $\text{Pb}(\text{OAc})_2(\text{Cu}(\text{salen}^*))$, and $[\text{Pb}(\text{OAc})(\text{Ni}(\text{salen}^*))_2](\text{OAc})$. *Inorg. Chem.* **2004**, *43*, 2708–2713. [[CrossRef](#)] [[PubMed](#)]
16. Kilic, A.; Tas, E.; Devenci, B.; Yilmaz, I. Synthesis, electrochemical and in situ spectroelectrochemical studies of new transition metal complexes with two new Schiff-bases containing $\text{N}_2\text{O}_2/\text{N}_2\text{O}_4$ donor groups. *Polyhedron* **2007**, *26*, 4009–4018. [[CrossRef](#)]
17. Biswas, R.; Ida, Y.; Baker, M.L.; Biswas, S.; Kar, P.; Nojiri, H.; Ishida, T.; Ghosh, A. A New Family of Trinuclear Nickel (II) Complexes as Single-Molecule Magnets. *Chem. Eur. J.* **2013**, *19*, 3943–3953. [[CrossRef](#)] [[PubMed](#)]
18. Hung, W.C.; Lin, C.C. Preparation, characterization, and catalytic studies of magnesium complexes supported by NNO-tridentate Schiff-base ligands. *Inorg. Chem.* **2008**, *48*, 728–734. [[CrossRef](#)] [[PubMed](#)]
19. Li, X.; Lah, M.S.; Pecoraro, V.L. Vanadium complexes of the tridentate Schiff base ligand N-salicylidene-N'-(2-hydroxyethyl) ethylenediamine: Acid-base and redox conversion between vanadium (IV) and vanadium (V) iminophenolates. *Inorg. Chem.* **1988**, *27*, 4657–4664. [[CrossRef](#)]
20. Mondal, M.; Guha, P.M.; Giri, S.; Ghosh, A. Deactivation of catecholase-like activity of a dinuclear Ni (II) complex by incorporation of an additional Ni (II). *J. Mol. Catal. A Chem.* **2016**, *424*, 54–64. [[CrossRef](#)]
21. Mukherjee, P.; Drew, M.G.B.; Gómez-García, C.J.; Ghosh, A. (Ni_2) , (Ni_3) , and $(\text{Ni}_2 + \text{Ni}_3)$: A Unique Example of Isolated and Cocrystallized Ni_2 and Ni_3 Complexes. *Inorg. Chem.* **2009**, *48*, 4817–4827. [[CrossRef](#)] [[PubMed](#)]
22. Adhikary, J.; Chakraborty, P.; Das, S.; Chattopadhyay, T.; Bauza, A.; Chattopadhyay, S.K.; Ghosh, B.; Mautner, F.A.; Frontera, A.; Das, D. A Combined Experimental and Theoretical Investigation on the Role of Halide Ligands on the Catecholase-like Activity of Mononuclear Nickel (II) Complexes with a Phenol-Based Tridentate Ligand. *Inorg. Chem.* **2013**, *52*, 13442–13452. [[CrossRef](#)] [[PubMed](#)]
23. Mondal, M.; Giri, S.; Guha, P.M.; Ghosh, A. Dependence of magnetic coupling on ligands at the axial positions of Ni^{II} in phenoxido bridged dimers: Experimental observations and DFT studies. *Dalton Trans.* **2017**, *46*, 697–708. [[CrossRef](#)] [[PubMed](#)]
24. Nanda, K.K.; Thompson, L.K.; Bridson, J.N.; Nag, K. Linear dependence of spin exchange coupling constant on bridge angle in phenoxy-bridged dinickel (II) complex. *J. Chem. Soc. Chem. Commun.* **1994**, *11*, 1337–1338. [[CrossRef](#)]
25. Burkhardt, A.; Spielberg, E.T.; Simon, S.; Görls, H.; Buchholz, A.; Plass, W. Hydrogen Bonds as Structural Directive towards Unusual Polynuclear Complexes: Synthesis, Structure, and Magnetic Properties of Copper (II) and Nickel (II) Complexes with a 2-Aminoglucose Ligand. *Chem. Eur. J.* **2009**, *15*, 1261–1271. [[CrossRef](#)] [[PubMed](#)]
26. Biswas, R.; Giri, S.; Saha, S.K.; Ghosh, A. One Ferromagnetic and Two Antiferromagnetic Dinuclear Nickel (II) Complexes Derived from a Tridentate N, N, O-Donor Schiff Base Ligand: A Density Functional Study of Magnetic Coupling. *Eur. J. Inorg. Chem.* **2012**, *2012*, 2916–2927. [[CrossRef](#)]
27. Banerjee, S.; Drew, M.G.B.; Lu, C.Z.; Tercero, J.; Diaz, C.; Ghosh, A. Dinuclear Complexes of M^{II} Thiocyanate ($\text{M} = \text{Ni}$ and Cu) Containing a Tridentate Schiff-Base Ligand: Synthesis, Structural Diversity and Magnetic Properties. *Eur. J. Inorg. Chem.* **2005**, *2005*, 2376–2383. [[CrossRef](#)]

28. Rodríguez, L.; Labisbal, E.; Sousa-Pedrares, A.; García-Vázquez, J.A.; Romero, J.; Durán, M.L.; Real, J.A.; Sousa, A. Coordination chemistry of amine bis (phenolate) cobalt (II), nickel (II), and copper (II) complexes. *Inorg. Chem.* **2006**, *45*, 7903–7914. [[CrossRef](#)] [[PubMed](#)]
29. Luo, W.; Wang, X.T.; Cheng, G.Z.; Gao, S.; Ji, Z.P. Synthesis, structural characterization, and magnetism of a butterfly-shaped hexanuclear Ni (II) complex. *Inorg. Chem. Commun.* **2008**, *11*, 769–771. [[CrossRef](#)]
30. Biswas, A.; Drew, M.G.B.; Gómez-García, C.J.; Ghosh, A. Formation of a dinuclear and a trinuclear Ni (II) complex on slight variation of experimental conditions: Structural analysis and magnetic properties. *Polyhedron* **2017**, *121*, 80–87. [[CrossRef](#)]
31. Ruiz, E.; Cano, J.; Alvarez, S.; Alemany, P. Magnetic coupling in end-on azido-bridged transition metal complexes: A density functional study. *J. Am. Chem. Soc.* **1998**, *120*, 11122–11129. [[CrossRef](#)]
32. Biswas, R.; Kar, P.; Song, Y.; Ghosh, A. The importance of an additional water bridge in making the exchange coupling of bis (μ -phenoxo) dinickel (II) complexes ferromagnetic. *Dalton Trans.* **2011**, *40*, 5324–5331. [[CrossRef](#)] [[PubMed](#)]
33. Biswas, R.; Diaz, C.; Ghosh, A. Three nickel (II) complexes derived from a tridentate NNO donor Schiff base ligand: Syntheses, crystal structures and magnetic properties. *Polyhedron* **2013**, *56*, 172–179. [[CrossRef](#)]
34. Mukherjee, P.; Drew, M.G.B.; Gomez-Garcia, C.J.; Ghosh, A. The crucial role of polyatomic anions in molecular architecture: Structural and magnetic versatility of five nickel (II) complexes derived from AN, N, O-donor schiff base ligand. *Inorg. Chem.* **2009**, *48*, 5848–5860. [[CrossRef](#)] [[PubMed](#)]
35. Mukherjee, P.; Drew, M.G.; Tangoulis, V.; Estrader, M.; Diaz, C.; Ghosh, A. Facile strategies for the synthesis and crystallization of linear trinuclear nickel (II)-Schiff base complexes with carboxylate bridges: Tuning of coordination geometry and magnetic properties. *Polyhedron* **2009**, *28*, 2989–2996. [[CrossRef](#)]
36. Romanović, M.Č.; Čobeljić, B.R.; Pevec, A.; Turel, I.; Spasojević, V.; Tsaturyan, A.A.; Shcherbakov, I.N.; Anđelković, K.K.; Milenković, M.; Radanović, D.; et al. Synthesis, crystal structure, magnetic properties and DFT study of dinuclear Ni(II) complex with the condensation product of 2-quinolinecarboxaldehyde and Girard's T reagent. *Polyhedron* **2017**, *128*, 30–37. [[CrossRef](#)]
37. Mahapatra, P.; Ghosh, S.; Giri, S.; Ghosh, A. The unusual intermediate species in the formation of Ni(II) complexes of unsymmetrical Schiff bases by Elder's method: Structural, electrochemical and magnetic characterizations. *Polyhedron* **2016**, *117*, 427–436. [[CrossRef](#)]
38. Blanchet-Boiteux, C.; Mouesca, J.M. End-on azido-bridged copper dimers: Spin population analysis and spin polarization effect as exhibited by valence-bond/broken symmetry, density functional methods. *J. Am. Chem. Soc.* **2000**, *122*, 861–869. [[CrossRef](#)]
39. Biswas, A.; Drew, M.G.; Diaz, C.; Bauzá, A.; Frontera, A.; Ghosh, A. Cis–trans isomerism in diphenoxido bridged dicopper complexes: Role of crystallized water to stabilize the cis isomer, variation in magnetic properties and conversion of both into a trinuclear species. *Dalton Trans.* **2012**, *41*, 12200–12212. [[CrossRef](#)] [[PubMed](#)]
40. Nanda, K.K.; Das, R.; Thompson, L.K.; Venkatsubramanian, K.; Paul, P.; Nag, K. Magneto-structural correlations in macrocyclic dinickel (II) complexes: Tuning of spin exchange by varying stereochemistry and auxiliary ligands. *Inorg. Chem.* **1994**, *33*, 1188–1193. [[CrossRef](#)]
41. Wang, C.; Fink, K.; Staemmler, V. A quantum chemical ab initio study of the superexchange coupling in binuclear oxygen-bridged Ni (II) complexes. *Chem. Phys.* **1995**, *192*, 25–35. [[CrossRef](#)]
42. Torić, F.; Pavlović, G.; Pajić, D.; Cindric, M.; Zadro, K. Tetranuclear Ni₄ cubane complexes with high χ T maxima: Magneto-structural analysis. *CrystEngComm* **2018**, *20*, 3917–3927. [[CrossRef](#)]
43. Bu, X.H.; Du, M.; Zhang, L.; Liao, D.Z.; Tang, J.K.; Zhang, R.H.; Shionoya, M. Anion-directed assembly: Framework conversion in dimensionality and photoluminescence. *J. Chem. Soc. Dalton Trans.* **2001**, *5*, 593–598. [[CrossRef](#)]
44. Biswas, A.; Das, L.K.; Drew, M.G.B.; Aromí, G.; Gamez, P.; Ghosh, A. Synthesis, crystal structures, magnetic properties and catecholase activity of double phenoxido-bridged penta-coordinated dinuclear nickel (II) complexes derived from reduced Schiff-base ligands: Mechanistic inference of catecholase activity. *Inorg. Chem.* **2012**, *51*, 7993–8001. [[CrossRef](#)] [[PubMed](#)]
45. Bain, G.A.; Berry, J.F. Diamagnetic corrections and Pascal's constants. *J. Chem. Educ.* **2008**, *85*, 532. [[CrossRef](#)]
46. Sheldrick, G.M. Shelxs97, Program for Crystallographic solution and refinement. *Acta Cryst.* **2008**, *A64*, 112. [[CrossRef](#)] [[PubMed](#)]
47. Sheldrick, G.M. Shelxl16/6, Program for Crystallographic Refinement. *Acta Cryst.* **2015**, *C71*, 3.

48. Platon, A.L. Spek. *Acta Cryst.* **2009**, *D65*, 148.
49. Noodleman, L. Valence bond description of antiferromagnetic coupling in transition metal dimers. *J. Chem. Phys.* **1981**, *74*, 5737–5743. [[CrossRef](#)]
50. Noodleman, L.; Case, D.A. Density-Functional Theory of Spin Polarization and Spin Coupling in Iron—Sulfur Clusters. *Adv. Inorg. Chem.* **1992**, *38*, 423–470.
51. Ruiz, E.; Rodríguez-Forteza, A.; Cano, J.; Alvarez, S.; Alemany, P. About the calculation of exchange coupling constants in polynuclear transition metal complexes. *J. Comput. Chem.* **2003**, *24*, 982–989. [[CrossRef](#)] [[PubMed](#)]
52. Becke, A.D. Becke's three parameter hybrid method using the LYP correlation functional. *J. Chem. Phys.* **1993**, *98*, 5648–5652. [[CrossRef](#)]
53. Lee, C.; Yang, W.; Parr, R.G. Development of the Colle-Salvetti correlation-energy formula into a functional of the electron density. *Phys. Rev. B* **1988**, *37*, 785. [[CrossRef](#)]
54. Becke, A.D. Density-functional exchange-energy approximation with correct asymptotic behavior. *Phys. Rev. A* **1988**, *38*, 3098. [[CrossRef](#)]
55. Schäfer, A.; Huber, C.; Ahlrichs, R. Fully optimized contracted Gaussian basis sets of triple zeta valence quality for atoms Li to Kr. *J. Chem. Phys.* **1994**, *100*, 5829–5835. [[CrossRef](#)]
56. Neese, F. The ORCA program system. *Wiley Interdiscip. Rev. Comput. Mol. Sci.* **2012**, *2*, 73–78. [[CrossRef](#)]
57. Giri, S.; Biswas, S.; Drew, M.G.B.; Ghosh, A.; Saha, S.K. Structure and magnetic properties of a tetranuclear Cu (II) complex containing the 2-(pyridine-2-yliminomethyl)-phenol ligand. *Inorg. Chim. Acta.* **2011**, *368*, 152–156. [[CrossRef](#)]
58. Weigend, F. Accurate Coulomb-fitting basis sets for H to Rn. *Phys. Chem. Chem. Phys.* **2006**, *8*, 1057–1065. [[CrossRef](#)] [[PubMed](#)]



© 2018 by the authors. Licensee MDPI, Basel, Switzerland. This article is an open access article distributed under the terms and conditions of the Creative Commons Attribution (CC BY) license (<http://creativecommons.org/licenses/by/4.0/>).